Setup to Study the In Situ Evolution of Both Photoluminescence and Absorption During the Processing of Organic or Hybrid Semiconductors

Michael Buchhorn[1], Stefan Wedler[1], Fabian Panzer[1*]

[1] Soft Matter Optoelectronics, University of Bayreuth, Bayreuth 95440, Germany.

Corresponding Author:

[*]E-Mail: fabian.panzer@uni-bayreuth.de

Abstract

In situ measurement techniques, applied during the solution processing of novel semiconductors such as organic semiconductors or hybrid perovskites, have become more and more important to understand their film formation. In that context, it is crucial to determine how the optical properties, namely photoluminescence (PL) and absorption, evolve during processing. However, until now PL and absorption have mostly been investigated independently, significantly reducing the potential insights into film formation dynamics. To tackle this issue we present the development of a detection system that allows simultaneous measurement of full absorption and PL spectra during solution processing of the investigated film. We also present a spin coater system attachable to the detection system, where the temperature of the substrate on which the film is processed can be changed. We performed test measurements by spin coating the well-known conjugated polymer P3HT demonstrating the potential of this technique. By considering absorption and corresponding PL, we extract the PL-Quantum Yield (PLQY) during processing, which decreases with substrate temperature. Furthermore, we identify a significant red shift of the PL just prior to the onset of the aggregation process, indicating the importance of chain-planarization prior to solid film formation.

Introduction:

Organic semiconductors and hybrid perovskites have emerged as highly important semiconductor materials, used as active layers in next generation optoelectronic devices including photovoltaics,[1-2] field effect transistors,[3-4] lighting and display devices,[5-6] and photodiodes for UV, visible[7-8] and high energy photons (e.g. X-Ray, gamma-ray).[9-11] For both types of semiconductor, changes in their local microstructure or morphology also impact their electronic structure, which significantly impacts the resulting performance of optoelectronic devices.[12-16] Such changes in structure and morphology naturally occur during the film formation from solution.[17-18] As electronic structure is highly dependent on local microstructure, optical properties also change. In recent years, this has led to the aim to track the optical properties of these materials during processing to monitor, better understand and finally control and optimize the film formation mechanisms.[19-20] This was achieved by controlling and systematically changing processing conditions such as atmosphere,[21] solvent,[22-23] or temperature.[24] The latter has an especially critical impact on film formation, as it not only influences the solvent drying rate, but also can dictate the conformational phase of the material prior and during film formation.[25]

In previous works, optical in situ detection was usually carried out by measuring absorption during processing. From these measurements it was possible to extract basic parameters, such as absorption coefficients and vibronic peak ratios, and to analyze how they evolve over time.[26-27]

However within the last years, several theoretical models and methodologies were developed that yield fundamental insights into underlying electronic structure requiring concurrent full absorption and photoluminescence (PL) spectra, ideally probing the same chromophore ensemble.[28-31] These studies could also provide fundamental insights on how changes in the electronic structure of the material correlate with their conformational and structural properties, even when they undergo significant changes, such as it is typically the case during processing or upon changing the temperature.[28-32]

However, these theoretical models cannot be readily applied to unravelling how interdependent processing conditions influence local microstructure and contingent optoelectronic properties, due to the difficulty inherent in collecting simultaneous PL and absorption spectra of the same region at a sufficently high frequency (> 10 Hz) to track the transition from solution to film. Pertinently, although such capability has been demonstrated for blade coating (albiet with absorption and PL probing adjacent locations),[33] this is not the case for the ubiquitous spin-coating film deposition method, limiting the scope of investigation into establishling the processing-structure-property relations essential in controlling device-relevant optelectonic properites.

In this work, we present an easy-to-use system for the quasi-simultaneous detection of absorption and photoluminescence during solution processing, including spin coating, of novel semiconductor materials such as π-conjugated polymers or hybrid perovskites. The system is designed to consist of only a few common optomechanical components and uses only one CCD-spectrograph for detection, which makes it portable, so it can be easily be combined with other in situ measurement techniques. Associated with this detection system, we also present a spin coater that allows for the detection of both absorption and PL during processing, probing the same region on the sample substrate. Furthermore, it is possible to control the substrate temperature during processing between 0°C and 150 C. With that, valuable insights on aggregate formation during the solution processing of the investigated material can be gained, which we demonstrate using the example of the polymer P3HT. This will help to tailor the route for processing next generation optoelectronic devices more expediently.

Experimental Setup:

Figure 1a shows a schematic representation of the spin coater device and in Figure 1b, an exploded view drawing of its 3D model is shown.

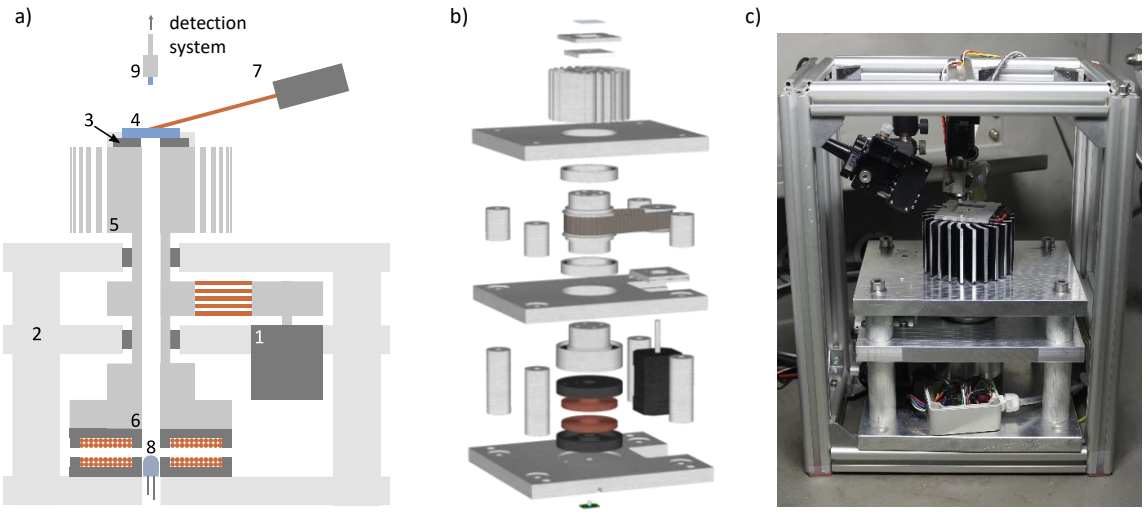

Figure 1: a) Schematic representation of the spin coater device. Relevant components are labeled by numbers, and described in more detail in the main text. b) Exploded View drawing of the spin coater device. c) Photograph of the assembled spin coater.

The main components are a brushless DC motor (**1**) (Trinamic BLDC4208) which is connected with the rotatable chuck via a cogged V-belt. In combination with a motor driver (Trinamic TMCM-1640) it is possible to set the rotation speed of up to 2300 rpm and control it via serial connection to a computer. To ensure balanced rotation, the chuck is mounted on two ball bearings, which are each edged into a robust aluminum structure (**2**). We use a Peltier element (**3**) to control the temperature of the substrate (**4**) on which the sample solution is deposited. It is located on a heat diffusor (**5**) in the upper part of the chuck. This passive heat exchanging geometry allows setting the substrate temperature between 0 – 150 °C and ensures quick thermal equilibration at the substrate. To allow heating and also cooling from room temperature, the Peltier's polarity can be

changed by a switch that is integrated in the chunk. The Peltier element can draw up to 60 W electrical power from a rotary transformer (**6**) after rectification, which is located at the lower part of the chuck. This approach reduces maintenances compared to the usage of slip rings, as no abrasion or corrosion can occur.

To allow quasi-simultaneous detection of both absorption and PL during processing, the spin coater setup is supplemented with a diode laser (**7**) above the substrate and a white LED (**8**). The latter is static and placed below the chuck. The type of the white LED can easily be changed, while we used a generic cold white LED covering a spectral range from 415 to about 820 nm (i.e. 1.51 – 2.99 eV) for our test measurements (*vide infra*). A bore along the rotation axis of the chuck with a diameter of 4 mm at the Peltier element allows the emitted white light to reach the substrate. Finally, the light transmitted through the substrate (and eventually the sample material) enters an optical fiber (**9**) above the sample that leads to the detection system.

The diode laser is attached to a frame made of common aluminum profiles. The laser's position can be chosen to ensure that the laser beam excites the top of the sample under a shallow angle to minimize self-absorption effects. We use a laser system that is based on exchangeable TO Can laser diodes, allowing us to choose excitation wavelengths between 405 and 820 nm (i.e. 1.51 – 3.07 eV). The emitted light from the sample enters the same optical fiber that is also used for the transmitted white light. Figure 1c shows a photograph of the entire spin coater device, including the frame with the diode laser.

The detection system to measure absorption and PL alternately is shown in Figure 2 and described below. To ensure a sufficient time resolution for tracking the optical properties during processing, we used only one spectrograph with CCD camera, and kept the spectral range between consecutive absorption and PL frames unchanged. We used a sufficiently large spectral range that includes the wavelength of the exciting laser, the absorption and the emission spectrum. This allows to subsequently also calculate the photoluminescence quantum yield (PL QY) as a function of film processing time, yet it requires to filter the

signal of the laser during the PL measurement to prevent damage of the CCD. For this purpose, we used two beam paths depending on whether absorption or PL is measured. In our detection system this is implemented by using a mechanical chopper with blades that have been coated to act as a mirror. Depending on the orientation of the chopper wheel (**1**), either a beam path for absorption (Figure 2a) or for PL (Figure 2b) is realized. For absorption, the transmitted light enters the detection system via the optical fiber (**2**) that is connected to the spin coater. A lens (**3**) collimates the light, which reaches the chopper wheel. The latter consists of two slots and the areas between them have a mirrored surface to reflect incident light. During an absorption measurement, the chopper wheel's orientation ensures a complete reflection of the collimated light. A lens (**4**) couples this reflected light into an optical fiber (**5**) connected to a spectrograph equipped with a CCD camera. For PL measurements, analogous to absorption, the emitted light from the sample enters the detection system through the optical fiber (**2**), is collimated by the lens (**3**) and reaches the chopper wheel (**1**). In contrast to absorption, the orientation of the chopper wheel ensures that incident light passes through a slot during a PL measurement. It further passes a filter (**6**) which is suitably selected to block the laser light. Using two mirrors (**7**, **8**), the filtered PL is then reflected back through the same slot of the chopper wheel, so that it matches the reflected light from the absorption measurement in terms of direction and position. This allows using the same lens (**4**) and optical fiber (**5**) to guide the PL signal to the same spectrograph. Due to its modular design, individual components of the detection system can easily be modified or exchanged to match particular sample requirements. This can for example concern the white light source to provide white light intensity over the relevant spectral range or the CCD spectrograph to meet the required sensitivity for detection when investigating different material systems with different optical properties.

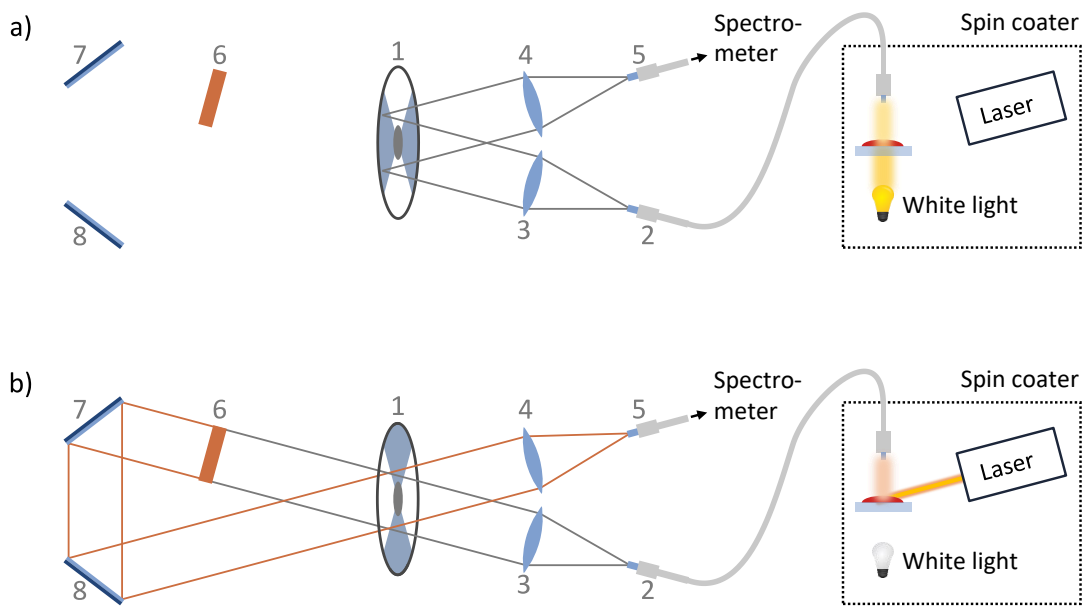

Figure 2: a) Schematic illustration of the main components of the detection system and corresponding operation states of the laser and white light during an absorption (a) and a PL (b) measurement. The different components are labeled by numbers and described in the main text.

A microcontroller (Atmel ATmega328p) ensures smooth interaction between the components that change their states depending on whether absorption or PL is measured. The microcontroller triggers absorption and PL measurements based on the orientation of the chopper wheel. During absorption measurements, the white LED is switched on while the laser diode is off, and vice versa for PL measurements. In each case, after LED and laser are set, the CCD camera is triggered to capture the corresponding spectrum. The maximum framerate for data collection is limited by the acquisition time of the CCD camera. It needs to be suitably chosen to ensure sufficient intensities for PL and absorption. We use homemade computer software to set acquisition settings of the CCD camera, to collect and visualize the data and to perform first analysis. The system proves to give excellent stabilities with fluctuations better than 0.3 % rms for the white LED intensity and 0.8 % rms for excitation intensity under typical measurement conditions.

Test Measurements:

To demonstrate the kind of information that can be obtained with this setup, we measured the absorption and emission during the drying process of the π-conjugated polymer poly(3-hexylthiophene) (P3HT), which is a well-established model system and has emerged as the workhorse in the organic semiconductor field over the last years. We spin coated P3HT from chlorobenzene solution with a concentration of 10 mg/ml, at a speed of 1000 rpm in a glovebox and measured the optical properties in situ, using our detection system (excitation intensity of 25 mW/cm^2 for PL) and spin coater. Figure 3 shows color-coded 2D-maps of time resolved absorption and corresponding PL spectra together with spectral slices at different times within the first 40 seconds of spin coating at room temperature (time resolution between two consecutive detection frames: 0.07 s). The intensities of the PL spectra are corrected for the changes of absorption at the laser excitation energy of 3.06 eV. Significant changes in both absorption and PL occur after 8-9 seconds, which are associated with the optical signatures of the well-known order-disorder transition, typically occurring upon P3HT film formation.[17, 34] This transition can also occur in solution upon lowering the quality of the solvent either by altering the temperature,[25, 35-36] or by systematically changing the ratio of good and bad solvents in solvent mixtures.[37-38]

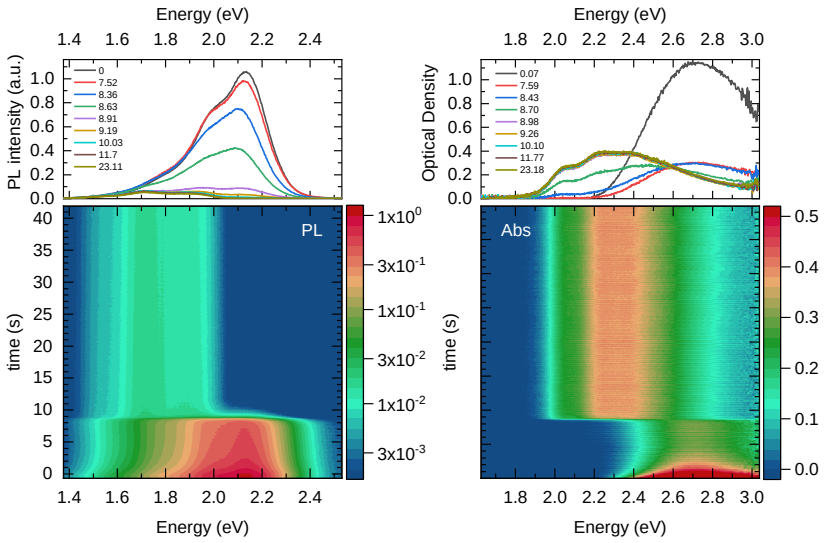

Figure 3: Photoluminescence (left) and absorbance (right) heat maps of P3HT taken at different times during spin coating from chlorobenzene solution at room temperature. In both cases time is displayed as ordinate and energy is displayed as abscissae. PL intensity and optical density are color coded. Horizontal cuts at the top of each heat map show spectra at certain times during processing.

Before the transition, i.e. within the first 8-9 seconds of spin coating, a broad and featureless absorption spectrum that is associated to the disordered phase of P3HT is observed, which reduces in intensity within the first 2 seconds of spin coating due to slinging away of excess solution upon rotation. Corresponding PL spectra within the first 8-9 seconds of spin coating are structured with a dominant peak at 2.13 eV that is attributed to PL from the disordered phase. This peak fully disappears in the course of the order-disorder-transition between 8 - 10 seconds. This is accompanied by the appearance of a red shifted PL spectrum of the aggregated phase with a non-dominant $S_1 \rightarrow S_0$ 0-0 peak at about 1.85 eV and by a significant reduction in overall PL intensity (note the logarithmic color code used in the 2D map of the PL). Both spectral changes are known spectroscopic signatures for the formation of an H-type intermolecular coupling within this phase.[39] In absorption, a red shifted, better-structured spectrum is the signature for the appearance of the aggregated phase. After 10 seconds, no significant spectral changes in both PL and absorption are observed from thereon until the end of the spin coating, indicating that the phase transition is complete.

We spin coated P3HT from CB solution also at 3 °C, 43 °C and 65 °C substrate temperature, while all other processing parameters were unchanged. We note that for the used temperatures the substrate temperature between the stationary state and upon rotation changes not more than 4 °C. 2D-maps of PL and absorption at the different processing temperatures during the spin coating are shown in Figure 4. The impact of substrate temperature on the onset time of the phase transition is obvious, with higher substrate temperatures leading to an earlier occurrence of the phase transition due to more rapid solvent evaporation.

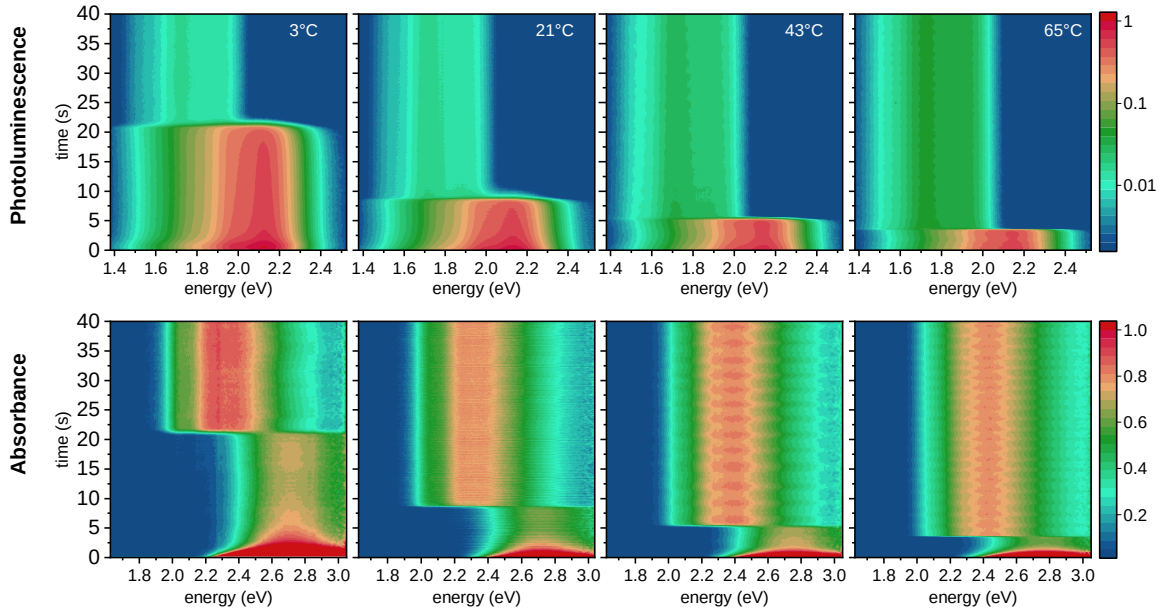

Figure 4: Normalized Photoluminescence (top) and absorption (bottom) heat maps of P3HT taken at different times during spin coating from chlorobenzene solution at 3 °C, 21 °C, 43 °C and 65 °C (from left to right). In each map time is displayed as ordinate and energy is displayed as abscissae. PL intensity and optical density are color coded. Time dependent fluctuations in the absorption intensity for 43 °C and 65 °C occur from inhomogeneous film distribution during spin coating.

This is consistent with a recent work from our group on in situ absorption measurements during spin coating of P3HT.[24] Furthermore, at higher temperatures, the initial drop in absorbance, due to the removal of material during spin coating, occurs more rapidly, which can be understood by considering the decreasing viscosity of chlorobenzene with temperature.[40]

As a first step, we extract parameters to identify and quantify the impact of processing temperature on the evolution of the optical properties. For this, we do not need to apply sophisticated models to the measured data. Rather, we exploit the fact that the absorption spectrum of the aggregated phase does not overlap with the absorption of the disordered phase at lower photon energies ($\lesssim$ 2.3 eV). Therefore, the intensity of the

peak at lowest energy i.e. 2.03 eV (associated with the $S_1 \leftarrow S_0$ 0-0 transition of the aggregated phase) can be taken to monitor the appearance and, to some extent, the amount of aggregated phase within the solution or film.[24, 26-27] Figure 5 top panel shows the normalized intensities at 2.03 eV for all four processing temperatures. From this we find the change of the onset time for the transition shifting from 21.1 s, 8.6 s, 5.3 s to 3.6 s for 3 °C, 21 °C, 43 °C to 65 °C respectively. We take the last frame before the steep increase of OD intensity at 2.03 eV (indicated as dashed lines in Figure 5) to determine the onset times for the film formation at each processing temperature. Furthermore, for 3 °C and 21 °C we find a small increase of the absorption intensity at 2.03 eV (to about 10 % of the maximum value) prior to the actual main transition, which indicates the formation of aggregates already in the solution drop on the substrate. Such a behavior can occur when the processing temperature is in the region of the critical order-disorder transition temperature T_c in solution,[24] where the longest polymer chains already aggregate due to the temperature dependence of T_c.[35, 41]

At first sight, the time dependent spectral changes of the PL spectra appear to correspond to the absorption spectra, as expected from temperature dependent spectroscopic studies in solution.[17, 25] However, plotting the energetic position of the $S_1 \rightarrow S_0$ 0-0 PL peak of the disordered phase as a function of spin coating time for all four processing temperatures (Figure 5 middle panel) reveals unexpected insights. First, the peak position at the beginning of spin coating increases with substrate temperature from 2.125 eV at 3°C to 2.146 eV at 65 °C. In the framework of the so-called oligomer approach, this shift is associated to a decrease in effective conjugation length. It is a known behavior for conjugated polymers in solution,[42] and the slope of this shift is in accordance with a recent publication.[43] As a function of processing time, the peak positions stay almost constant at the beginning, but start to shift to lower energies close before the onset of each phase transition. We could clearly determine each onset from the analysis of the absorption spectra as described above (indicated with dashed lines in Figure 5).

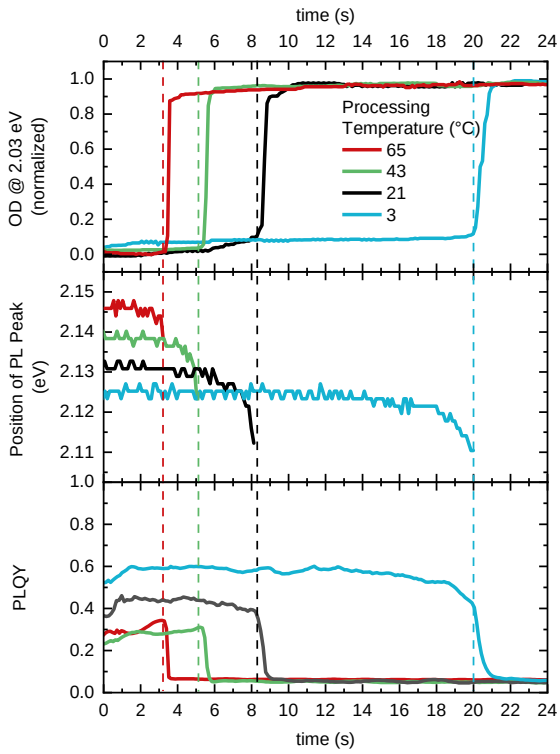

Figure 5: Evolution of relevant parameters during spin coating at different temperatures, extracted from the time resolved absorption and PL data. Top panel: Optical density at 2.03 eV, which is associated to absorption from aggregated phase. Middle panel: The PL peak position in the time range prior to film formation. Bottom panel: PLQY, calculated from the evolution of integrated PL intensity, corrected for the changes of optical density at 3.05 eV and scaled with absolute PLQY values of the final thin films. The onset times are shown as dashed vertical lines.

We find that the amount of red shift of the PL spectrum between the start of spin coating and the onset of the phase transition is lower for higher processing temperatures. The reason for the red shift could be due to an increase in conjugation length of the disordered chains in the course of a chain planarization (pre-aggregation) prior to the main order-disorder transition. It could also be influenced by a changing polarization environment of the polymer chains close before the phase transition, which would also impact on the electronic structure and result in a spectral shift.[17]

Additionally, the quasi-simultaneous detection of absorption and PL further allows extracting the relative change of absorbed light at the laser excitation wavelength during processing, which then can be used to scale the time dependent integrated PL intensity. The resulting value represents the relative change of the PLQY. In addition, we determined the absolute PLQY values following the approach by de Mello et al.[44] We find them to be in the range between 3-5 % for all films, which is consistent with typical values for P3HT thin films.[45] Using the absolute values of the PLQY of each final film also enables the absolute change of the PLQY during spin coating to be determined for the different processing temperatures (Figure 5 bottom panel).

We followed this approach and find that the PLQY reduces significantly during film formation for all investigated samples. Prior to the formation of aggregates, we find that the PLQY values reduce from almost 60 % for 3° C to about 40 % at room temperature and about 30 % for both 43 and 65 °C. This temperature dependence of PLQY of the disordered phase was also observed for different π-conjugated material systems in the past. It results from an increased conjugation length due to a reduction of (thermally activated) torsional disorder and an decreased solubility at lower temperatures.[25] Furthermore, the absolute value of about 40 % at room temperature is consistent with literature values reported for disordered P3HT in solution.[45] The PLQYs at room temperature and 3 °C stay relatively constant until film formation sets in, while the PLQYs for 43 °C and 65 °C show an additional increase shortly before the phase transition. We speculate that an efficient energy transfer from disordered chains to the small fraction of already existing aggregated chains might mask this increase in PLQY for the lower processing temperatures. However a full investigation of this behavior and the physical origin of the spectral red shift prior to aggregation will be focus of an in-depth study in the future.

Conclusion and Outlook

In conclusion, we have presented a detection system that is able to measure the absorption and the PL of semiconductor materials during their solution processing in an alternating shot-by-shot manner, probing the same sample region. Furthermore, we presented a newly designed spin coater compatible with the detection system, where the substrate temperature can be set or changed even while spinning. Together, this system allows correlating the time evolution of absorption and PL spectra during processing at different substrate temperatures, allowing for example the extraction of important optoelectronic parameters such as PLQY. Using this setup allowed us to identify a significant red shift of the PL spectrum of the disordered phase prior to aggregate formation in test measurements of the polymer P3HT. This underlines the importance of chain planarization before the main aggregation process. We could extract the evolution of the PLQY during processing of P3HT for different substrate temperatures in the range between 3 °C and 65 °C, where we find increased PLQY values for lower processing temperatures in the time range before film formation. These results demonstrate the high potential of the setup to gain new fundamental insights into the film formation processes of solution processed novel semiconductors, which will help to optimize their film formation.

As an outlook, our approach to simultaneous in situ PL and absorption measurement could be easily extended to other thin film processing techniques, particularly those relevant for large-area production such as blade coating, slot-dye coating or ink-jet printing. Systematically comparing film formation dynamics across processing methods will assist in understanding why local microstructure and resulting macroscopic optoelectronic properties shows such a pronounced deposition method dependence, an especially important goal given that organic or hybrid optoelectronic devices produced with scalable methods are typically significantly less efficient than those with a spin-coated active layer. To extract more information about the electronic structure from the

PL and absorption spectra, theoretical models such as multi-mode Franck-Condon-Analysis could be globally applied. The setup also easily allows investigating the changes of optical properties that occur when a semiconductor material undergoes a crystallization process upon cooling from the melt or vice versa. Furthermore, as the presented spin coater provides electrical power even during rotation, extensions regarding additional sensing on the chuck could be realized easily and electrical fields could be provided during processing, where the positive impact of the latter on film formation has been proven recently.[46-48] The aim to combine different in situ measurement techniques during the processing has gained momentum within the last few years,[49-50] especially involving in situ scattering techniques such as GIWAXS or GISAXS.[51-54] As the latter can yield detailed information about structure formation on the micro- and the mesoscale, a combination of these techniques with the detection system presented here would yield the possibility to directly correlate conformational changes with changes in the optical properties of the investigated material and is a promising future direction for in situ real time investigations during processing.

Acknowledgement

We thank Frank Schirmer and Thomas Dabisch for technical help with the setup, Anna Köhler, Eva Herzig and Matt Dyson for fruitful discussions, and the mechanic and the electronic workshop of the University for supporting the development of the setup. F.P. acknowledges support from the Marie-Curie Innovative Training Network (ITN) INFORM. Financial support is acknowledged from the Deutsche Forschungsgemeinschaft through GRK1640 (Photophysics of Synthetic and Biological Multichromophoric Systems) and from the Bayerisches Staatsministerium für Bildung und Kultus, Wissenschaft und Kunst through the grant “Solar Technologies go Hybrid” as well as the program “MINT-Lehramt plus”.

References

1. Brabec, C. J.; Gowrisanker, S.; Halls, J. J.; Laird, D.; Jia, S.; Williams, S. P. Polymer-Fullerene Bulk-Heterojunction Solar Cells. *Adv. Mater.* **2010,** *22*, 3839-3856.
2. Hedley, G. J.; Ruseckas, A.; Samuel, I. D. W. Light Harvesting for Organic Photovoltaics. *Chem. Rev.* **2017,** *117*, 796-837.
3. Sirringhaus, H. 25th Anniversary Article: Organic Field-Effect Transistors: The Path Beyond Amorphous Silicon. *Adv. Mater.* **2014,** *26*, 1319-1335.
4. Torsi, L.; Magliulo, M.; Manoli, K.; Palazzo, G. Organic Field-Effect Transistor Sensors: A Tutorial Review. *Chem. Soc. Rev.* **2013,** *42*, 8612-8628.
5. Bhatnagar, P. K. Organic Light-Emitting Diodes—A Review. In *Nanomaterials and Their Applications*; Khan, Z. H. Ed.; Springer Singapore: Singapore, 2018; pp 261-287.
6. Xu, R.-P.; Li, Y.-Q.; Tang, J.-X. Recent Advances in Flexible Organic Light-Emitting Diodes. *J. Mater. Chem. C* **2016,** *4*, 9116-9142.
7. Jansen-van Vuuren, R. D.; Armin, A.; Pandey, A. K.; Burn, P. L.; Meredith, P. Organic Photodiodes: the Future of Full Color Detection and Image Sensing. *Adv. Mater.* **2016,** *28*, 4766-4802.
8. Baeg, K. J.; Binda, M.; Natali, D.; Caironi, M.; Noh, Y. Y. Organic Light Detectors: Photodiodes and Phototransistors. *Adv. Mater.* **2013,** *25*, 4267-4295.
9. Shrestha, S.; Fischer, R.; Matt, G. J.; Feldner, P.; Michel, T.; Osvet, A.; Levchuk, I.; Merle, B.; Golkar, S.; Chen, H. et al. High-Performance Direct Conversion X-Ray Detectors Based on Sintered Hybrid Lead Triiodide Perovskite Wafers. *Nat. Photonics* **2017,** *11*, 436.
10. Benavides, C. M.; Murto, P.; Chochos, C. L.; Gregoriou, V. G.; Avgeropoulos, A.; Xu, X.; Bini, K.; Sharma, A.; Andersson, M. R.; Schmidt, O. et al. High-Performance Organic Photodetectors from a High-Bandgap Indacenodithiophene-Based π-Conjugated Donor–Acceptor Polymer. *ACS Appl. Mater. Interfaces* **2018,** *10*, 12937-12946.
11. Büchele, P.; Richter, M.; Tedde, S. F.; Matt, G. J.; Ankah, G. N.; Fischer, R.; Biele, M.; Metzger, W.; Lilliu, S.; Bikondoa, O. et al. X-ray Imaging with Scintillator-Sensitized Hybrid Organic Photodetectors. *Nat. Photonics* **2015,** *9*, 843.
12. Sirringhaus, H.; Brown, P. J.; Friend, R. H.; Nielsen, M. M.; Bechgaard, K.; Langeveld-Voss, B. M. W.; Spiering, A. J. H.; Janssen, R. A. J.; Meijer, E. W.; Herwig, P. et al.Two-Dimensional Charge Transport in Self-Organized, High-Mobility Conjugated Polymers. *Nature* **1999,** *401*, 685.
13. Schubert, M.; Dolfen, D.; Frisch, J.; Roland, S.; Steyrleuthner, R.; Stiller, B.; Chen, Z.; Scherf, U.; Koch, N.; Facchetti, A. et al. Influence of Aggregation on the Performance of All-Polymer Solar Cells Containing Low-Bandgap Naphthalenediimide Copolymers. *Adv. Energy Mater.* **2012,** *2*, 369-380.
14. Duong, D. T.; Ho, V.; Shang, Z.; Mollinger, S.; Mannsfeld, S. C. B.; Dacuña, J.; Toney, M. F.; Segalman, R.; Salleo, A. Mechanism of Crystallization and Implications for Charge Transport in Poly(3-ethylhexylthiophene) Thin Films. *Adv. Funct. Mater.* **2014,** *24*, 4515-4521.
15. Liu, Y.; Zhao, J.; Li, Z.; Mu, C.; Ma, W.; Hu, H.; Jiang, K.; Lin, H.; Ade, H.; Yan, H. Aggregation and Morphology Control Enables Multiple Cases of High-Efficiency Polymer Solar Cells. *Nat. Commun* **2014,** *5*, 5293.
16. Noriega, R.; Rivnay, J.; Vandewal, K.; Koch, F. P. V.; Stingelin, N.; Smith, P.; Toney, M. F.; Salleo, A. A General Relationship Between Disorder, Aggregation and Charge Transport in Conjugated Polymers. *Nat. Mater* **2013,** *12*, 1038.
17. Hildner, R.; Köhler, A.; Müller-Buschbaum, P.; Panzer, F.; Thelakkat, M. π-Conjugated Donor Polymers: Structure Formation and Morphology in Solution, Bulk and Photovoltaic Blends. *Adv. Energy Mater.* **2017,** *7*, 1700314.
18. Guilbert, A. A. Y.; Cabral, J. T. Impact of Solution Phase Behaviour and External Fields on Thin Film Morphology: PCBM and RRa-P3HT Model System. *Soft Matter* **2017,** *13*, 827-835.

19. Güldal, N. S.; Kassar, T.; Berlinghof, M.; Unruh, T.; Brabec, C. J. In Situ Characterization Methods for Evaluating Microstructure Formation and Drying Kinetics of Solution-Processed Organic Bulk-Heterojunction Films. *J. Mater. Res.* **2017,** *32*, 1855-1879.
20. Richter, L. J.; DeLongchamp, D. M.; Amassian, A. Morphology Development in Solution-Processed Functional Organic Blend Films: An In Situ Viewpoint. *Chem. Rev.* **2017,** *117*, 6332-6366.
21. Pröller, S.; Mosegui Gonzalez, D.; Zhu, C.; Schaible, E.; Wang, C.; Müller-Buschbaum, P.; Hexemer, A.; Herzig, E. M. Note: Setup for Chemical Atmospheric Control During In Situ Grazing Incidence X-Ray Scattering of Printed Tin Flms. *Rev. Sci. Instrum.* **2017,** *88*, 066101.
22. Chang, J.-F.; Sun, B.; Breiby, D. W.; Nielsen, M. M.; Sölling, T. I.; Giles, M.; McCulloch, I.; Sirringhaus, H. Enhanced Mobility of Poly(3-hexylthiophene) Transistors by Spin-Coating from High-Boiling-Point Solvents. *Chem. Mater.* **2004,** *16*, 4772-4776.
23. Park, Y. D.; Lee, H. S.; Choi, Y. J.; Kwak, D.; Cho, J. H.; Lee, S.; Cho, K. Solubility-Induced Ordered Polythiophene Precursors for High-Performance Organic Thin-Film Transistors. *Adv. Funct. Mater.* **2009,** *19*, 1200-1206.
24. Reichenberger, M.; Kroh, D.; Matrone, G. M. M.; Schötz, K.; Pröller, S.; Filonik, O.; Thordardottir, M. E.; Herzig, E. M.; Bässler, H.; Stingelin, N. et al. Controlling Aggregate Formation in Conjugated Polymers by Spin-Coating Below the Critical Temperature of the Disorder-Order Transition. *J. Polym. Sci., Part B: Polym. Phys.* **2018,** *56*, 532-542.
25. Panzer, F.; Bassler, H.; Kohler, A. Temperature Induced Order-Disorder Transition in Solutions of Conjugated Polymers Probed by Optical Spectroscopy. *J. Phys. Chem. Lett.* **2017,** *8*, 114-125.
26. Abdelsamie, M.; Zhao, K.; Niazi, M. R.; Chou, K. W.; Amassian, A. In Situ UV-Visible Absorption During Spin-Coating of Organic Semiconductors: A New Probe for Organic Electronics and Photovoltaics. *J. Mater. Chem. C* **2014,** *2*, 3373-3381.
27. Reichenberger, M.; Baderschneider, S.; Kroh, D.; Grauf, S.; Köhler, J.; Hildner, R.; Köhler, A. Watching Paint Dry: The Impact of Diiodooctane on the Kinetics of Aggregate Formation in Thin Films of Poly(3-hexylthiophene). *Macromolecules* **2016,** *49*, 6420-6430.
28. Spano, F. C.; Silva, C. H- and J-Aggregate Behavior in Polymeric Semiconductors. *Annu. Rev. Phys. Chem.* **2014,** *65*, 477-500.
29. Yamagata, H.; Spano, F. C. Interplay Between Intrachain and Interchain Interactions in Semiconducting Polymer Assemblies: The HJ-Aggregate Model. *J. Chem. Phys.* **2012,** *136*, 184901.
30. Spano, F. C. The Spectral Signatures of Frenkel Polarons in H- and J-Aggregates. *Acc. Chem. Res.* **2010,** *43*, 429-439.
31. Barford, W.; Marcus, M. Perspective: Optical Spectroscopy in π-conjugated Polymers and How it can be Used to Determine Multiscale Polymer Structures. *J. Chem. Phys.* **2017,** *146*, 130902.
32. Köhler, A.; Bässler, H. In *Electronic Processes in Organic Semiconductors*; Köhler, A.; Bässler, H., Eds.; Wiley-VCH, 2015, pp 1-86
33. Engmann, S.; Bokel, F. A.; Ro, H. W.; DeLongchamp, D. M.; Richter, L. J. Real-Time Photoluminescence Studies of Structure Evolution in Organic Solar Cells. *Adv. Energy Mater.* **2016,** *6*, 1502011.
34. Brown, P. J.; Thomas, D. S.; Köhler, A.; Wilson, J. S.; Kim, J.-S.; Ramsdale, C. M.; Sirringhaus, H.; Friend, R. H. Effect of Interchain Interactions on the Absorption and Emission of Poly(3-hexylthiophene). *Phys. Rev. B* **2003,** *67*, 064203.
35. Panzer, F.; Bässler, H.; Lohwasser, R.; Thelakkat, M.; Köhler, A. The Impact of Polydispersity and Molecular Weight on the Order–Disorder Transition in Poly(3-hexylthiophene). *J. Phys. Chem. Lett.* **2014,** *5*, 2742-2747.
36. Panzer, F.; Sommer, M.; Bässler, H.; Thelakkat, M.; Köhler, A. Spectroscopic Signature of Two Distinct H-Aggregate Species in Poly(3-hexylthiophene). *Macromolecules* **2015,** *48*, 1543-1553.
37. Bockmann, M.; Schemme, T.; de Jong, D. H.; Denz, C.; Heuer, A.; Doltsinis, N. L. Structure of P3HT Crystals, Thin Films, and Solutions by UV/Vis Spectral Analysis. *PCCP* **2015,** *17*, 28616-28625.

38. Scharsich, C.; Lohwasser, R. H.; Sommer, M.; Asawapirom, U.; Scherf, U.; Thelakkat, M.; Neher, D.; Köhler, A. Control of Aggregate Formation in Poly(3-hexylthiophene) by Solvent, Molecular Weight, and Synthetic Method. *J. Polym. Sci., Part B: Polym. Phys.* **2012,** *50*, 442-453.
39. Clark, J.; Silva, C.; Friend, R. H.; Spano, F. C. Role of Intermolecular Coupling in the Photophysics of Disordered Organic Semiconductors: Aggregate Emission in Regioregular Polythiophene. *Phys. Rev. Lett.* **2007,** *98*, 206406.
40. Haase, R.; Lethen, M.; Dücker, K. H. Viskosität des flüssigen Systems Chlorbenzol + Brombenzol. In *Z. Naturforsch., A: Phys. Sci.*, **1975**, 30, 916.
41. Cone, C. W.; Cheng, R. R.; Makarov, D. E.; Vanden Bout, D. A. Molecular Weight Effect on the Formation of β Phase Poly(9,9′-dioctylfluorene) in Dilute Solutions. *J. Phys. Chem. B* **2011,** *115*, 12380-12385.
42. Köhler, A.; Bässler, H. In *Electronic Processes in Organic Semiconductors*; Köhler, A.; Bässler, H., Eds.; Wiley-VCH, 2015, pp 87-191
43. Raithel, D.; Simine, L.; Pickel, S.; Schötz, K.; Panzer, F.; Baderschneider, S.; Schiefer, D.; Lohwasser, R.; Köhler, J.; Thelakkat, M. et al. Direct Observation of Backbone Planarization via Side-Chain Alignment in Single Bulky-Substituted Polythiophenes. *Proc. Natl. Acad. Sci. U.S.A.* **2018,** *115*, 2699-2704.
44. de Mello, J. C.; Wittmann, H. F.; Friend, R. H. An Improved Experimental Determination of External Photoluminescence Quantum Efficiency. *Adv. Mater.* **1997**, 9, 230-232
45. Cook, S.; Furube, A.; Katoh, R. Analysis of the Excited States of Regioregular Polythiophene P3HT. *Energy Environ. Sci.* **2008,** *1*, 294-299.
46. Solanki, A.; Bagui, A.; Long, G.; Wu, B.; Salim, T.; Chen, Y.; Lam, Y. M.; Sum, T. C. Effectiveness of External Electric Field Treatment of Conjugated Polymers in Bulk-Heterojunction Solar Cells. *ACS Appl. Mater. Interfaces* **2016,** *8*, 32282-32291.
47. Elshobaki, M.; Gebhardt, R.; Carr, J.; Lindemann, W.; Wang, W.; Grieser, E.; Venkatesan, S.; Ngo, E.; Bhattacharjee, U.; Strzalka, J. et al. Tailoring Nanoscale Morphology of Polymer:Fullerene Blends Using Electrostatic Field. *ACS Appl. Mater. Interfaces* **2017,** *9*, 2678-2685.
48. Molina-Lopez, F.; Yan, H.; Gu, X.; Kim, Y.; Toney, M. F.; Bao, Z. Electric Field Tuning Molecular Packing and Electrical Properties of Solution-Shearing Coated Organic Semiconducting Thin Films. *Adv. Funct. Mater.* **2017,** *27*, 1605503.
49. Guldal, N. S.; Kassar, T.; Berlinghof, M.; Ameri, T.; Osvet, A.; Pacios, R.; Li Destri, G.; Unruh, T.; Brabec, C. J. Real-Time Evaluation of Thin Film Drying Kinetics Using an Advanced, Multi-Probe Optical Setup. *J. Mater. Chem. C* **2016,** *4*, 2178-2186.
50. Alsari, M.; Bikondoa, O.; Bishop, J.; Abdi-Jalebi, M.; Y. Ozer, L.; Hampton, M.; Thompson, P.; T. Horantner, M.; Mahesh, S.; Greenland, C. et al. In Situ Simultaneous Photovoltaic and Structural Evolution of Perovskite Solar Cells During Film Formation. *Energy Environ. Sci.* **2018,** *11*, 383-393.
51. Yoo, E. J.; Lyu, M.; Yun, J. H.; Kang, C. J.; Choi, Y. J.; Wang, L. Resistive Switching Behavior in Organic-Inorganic Hybrid $CH_3NH_3PbI_{3-x}Cl_x$ Perovskite for Resistive Random Access Memory Devices. *Adv. Mater.* **2015,** *27*, 6170-6175.
52. Pröller, S.; Liu, F.; Zhu, C.; Wang, C.; Russell, T. P.; Hexemer, A.; Müller-Buschbaum, P.; Herzig, E. M. Following the Morphology Formation In Situ in Printed Active Layers for Organic Solar Cells. *Adv. Energy Mater.* **2016,** *6*, 1501580.
53. van Franeker, J. J.; Hermida-Merino, D.; Gommes, C.; Arapov, K.; Michels, J. J.; Janssen, R. A. J.; Portale, G. Sub-Micrometer Structure Formation during Spin Coating Revealed by Time-Resolved In Situ Laser and X-Ray Scattering. *Adv. Funct. Mater.* **2017,** *27*, 1702516.
54. Manley, E. F.; Strzalka, J.; Fauvell, T. J.; Jackson, N. E.; Leonardi, M. J.; Eastham, N. D.; Marks, T. J.; Chen, L. X. In Situ GIWAXS Analysis of Solvent and Additive Effects on PTB7 Thin Film Microstructure Evolution during Spin Coating. *Adv. Mater.* **2017,** *29*, 1703933.

TOC Graphic:

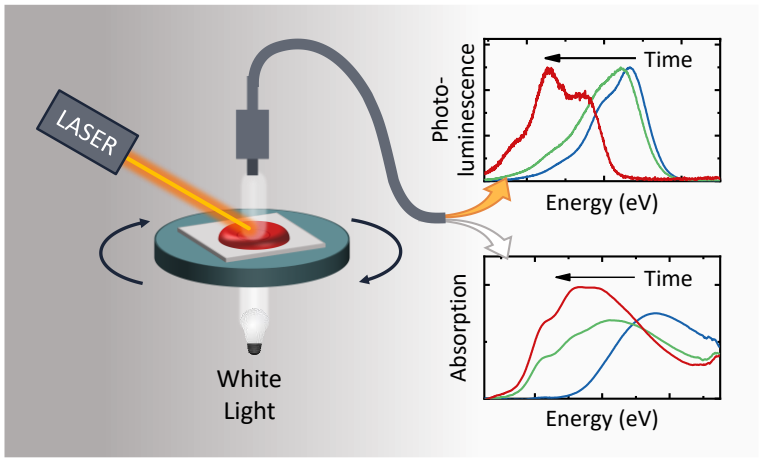
LASER
White
Light
Photo-
luminescence
Time
Energy (eV)
Absorption
Time
Energy (eV)